SAND2019-0133C

# Benchmarking and QA testing in PFLOTRAN

Tara LaForce, Jennifer M. Frederick, Glenn E. Hammond, Emily R. Stein, Paul E. Mariner

*Sandia National Laboratories: P.O. Box 5800, Albuquerque, NM and tara.laforce@sandia.gov*

*PFLOTRAN is well-established in single-phase reactive transport problems, and current research is expanding its visibility and capability in two-phase subsurface problems. A critical part of the development of simulation software is quality assurance (QA). The purpose of the present work is QA testing to verify the correct implementation and accuracy of two-phase flow models in PFLOTRAN. An important early step in QA is to verify the code against exact solutions from the literature.*

*In this work a series of QA tests on models that have known analytical solutions are conducted using PFLOTRAN. In each case the simulated saturation profile is rigorously shown to converge to the exact analytical solution. These results verify the accuracy of PFLOTRAN for use in a wide variety of two-phase modelling problems with a high degree of nonlinearity in the interaction between phase behavior and fluid flow.*

## I. INTRODUCTION

Benchmarking of codes against analytical solutions is a key part of code development, as it allows developers to verify that the simulation converges to the correct solution for simplified problems. Analytical solutions are typically too simple to be representative of realistic scenarios in the subsurface, however if each part of the equations used in a complex simulation have been demonstrated to provide the correct solution, confidence can be gained that the full set of equations are implemented correctly and accurately. Code benchmarking is especially important if the software is used to model high-consequence systems which cannot be physically tested in a fully representative environment (Oberkampf and Trucano 2007), such as the performance assessment of a geologic nuclear waste repository.

PFLOTRAN, an open source, massively parallel subsurface flow and reactive transport code, is part of a software toolkit, Geologic Disposal Safety Assessment (GDSA) Framework, under development by the U.S. Department of Energy (DOE) for performance assessment of deep geologic repositories for nuclear waste. The DOE is considering direct disposal of large dual-purpose canisters (DPCs) containing spent nuclear fuel. Assuming 150-year storage of high burn-up fuel, heat output at the time of disposal can be sufficient to boil in situ pore water. Reactions of the canister may also generate hydrogen gas. This necessitates inclusion of high-temperature two-phase flow in simulations of DPC disposal.

Beginning in FY2017, a new QA testing suite was developed to perform code verification for several basic processes in PFLOTRAN (Mariner et al. 2017). The testing suite consists of more than 50 individual tests exercising single-phase fluid flow, heat transfer, and radionuclide decay and ingrowth. The purpose of the present work is verification of the accuracy of two-phase flow models in PFLOTRAN.

One-dimensional analytical models are particularly useful in verifying that a simulator is accurately modelling chemo-physical processes such as the nonlinear interaction of multiple phases flowing simultaneously and the transition of chemical components between phases during flow. These processes are typically too complex to allow for analytical solutions in multiple dimensions.

In this work a series of QA tests on one-dimensional models that have known analytical solutions are conducted in PFLOTRAN. One-dimensional simulations of injection of an immiscible, isothermal fluid to displace water (called the Buckley-Leverett problem in petroleum engineering) are conducted. It is shown that the simulated fluid profile converges to the analytical solution as the mesh is refined. Subsequently more complex variations of the Buckley-Leverett problem are modelled including: radial geometry, component partitioning between the phases and injection of a cold fluid. In each case the simulated saturation profile is rigorously shown to converge to the analytical solution.

These results verify the accuracy of PFLOTRAN for use in two-phase modelling problems. The suite of QA problems are publicly available as an option in the suite of QA tests available for PFLOTRAN at https://qa.pflotran.org.

Sandia National Laboratories is a multimission laboratory managed and operated by National Technology & Engineering Solutions of Sandia, LLC, a wholly owned subsidiary of Honeywell International Inc., for the U.S. Department of Energy's National Nuclear Security Administration under contract DE-NA0003525.

## II. VERIFICATION AGAINST ANALYTICAL SOLUTIONS

The method of characteristics (MOC) can be used to find travelling wave solutions for purely advective multiphase, multicomponent flow through an incompressible porous media. The model applies to constant rate injection of an incompressible fluid into a porous media containing constant saturation of a second incompressible fluid with which it is immiscible or slightly miscible. The temperature of the injected fluid may be different than the porous medium, however the temperature of both must be constant with respect to time.

A general model for two-component, two-phase flow that can be solved using MOC is (Orr, 2007; Lake 1989, Sumnu-Dindoruk and Dindoruk, 2008):

$$\varphi \frac{\partial C_i}{\partial t} + v \frac{\partial F_i}{\partial x} = 0 \tag{1}$$

$$\frac{\partial T}{\partial t} + g \frac{\partial T}{\partial x} = 0 \tag{2}$$

with auxiliary relations

$$C_i = \sum_{j=1}^{2} c_{ij} \rho_j S_j \qquad F_i = \sum_{j=1}^{2} c_{ij} \rho_j f_j \tag{3}$$

$$f_j = \frac{k_{rj}/\mu_j}{k_{r1}/\mu_1 + k_{r2}/\mu_2} \tag{4}$$

$$g = \frac{f_1 + \alpha}{S_1 + \beta} \qquad \alpha = \frac{\rho_2 c_{v2}}{\rho_1 c_{v1} - \rho_2 c_{v2}} \qquad \beta = \frac{\rho_2 c_{v2} + \frac{1-\varphi}{\varphi} \rho_r c_{vr}}{\rho_1 c_{v1} - \rho_2 c_{v2}} \tag{5}$$

where $C_i$ is the molar concentration of component i, $F_i$ is the molar flow of component i, $S_j$, $f_j$, $k_{rj}$, $\rho_j$, and $\mu_j$ are the saturation, fractional flow, relative permeability, density, and viscosity of phase j, $c_{ij}$ is the mole fraction of component i in phase j, $c_{jv}$ is the heat capacity of the fluid or rock. Time is denoted by t, T is temperature and $\phi$ is porosity. The distance from the injection point is denoted x, and may be either linear or radial distance.

Table 1 describes the analytical models that PFLOTRAN is tested against in the present work. A full discussion of the analytical solutions to these equations is beyond the scope of this paper, however references to detailed discussions for each case are included in every subsection, and python scripts to solve each benchmark case are available at https://qa.pflotran.org.

The system of equations outlined in Eq. 1-5 is quite challenging from a numerical perspective. The system of equations of purely advective flow with no capillary pressure and incompressible fluids and solids is numerically very stiff. The solutions also admit shocks in saturation and temperature which must be numerically resolved. This results in simulators having to take small timesteps and simulation times that are much longer than one might expect for such small one-dimensional problems. Moreover, previous studies have shown that for multi-phase flow problems convergence rates are at best first-order (Goater and LaForce, 2010).

### I.A. Model 1: Immiscible, isothermal linear flow

In petroleum engineering literature the model for isothermal flow of two completely immiscible fluids is known as the Buckley-Leverett problem. Model 1 is used to explore the nonlinearities introduced by having two phases, each with relative permeability $k_{rj}(S_j)$ where the $k_{rj}$ are typically a polynomial function of $S_j$. For the case of isothermal injection from a point source in one dimension and two immiscible phases the model in Eq. 1-2 simplifies to:

$$\varphi \frac{\partial S_j}{\partial t} + v \frac{\partial f_j}{\partial x} = 0 \tag{6}$$

where $C_1=S_1$ and $f_j$ is defined in auxiliary relation Eq. 4. In this case the thermal equation is not needed, as temperature is the same everywhere.

MOC gives a travelling wave solution to Eq. 1 where the wave velocity is proportional to x/t. Lake (1989) section 5.2 shows examples of the construction of solutions for this kind of model. The solution consists of a shock where the gas saturation changes from zero to an intermediate value, followed by a rarefaction curve or spreading wave where the gas saturation gradually increases to $1-S_{wr}$.

Model 1 represents injection of an ideal gas at 1 atm and 25°C into an aquifer completely saturated with water. Gas injection takes place at x=0, and the aquifer is modelled as 10 m long, but has an open boundary at x=10m to represent an infinite-acting aquifer. The parameters used in this test are outlined in Table 2.

The phases are made to behave immiscibly and isothermally by using the IMMISCIBLE and ISOTHERMAL keywords in PFLOTRAN. The built-in Burdine/Brooks-Corey relative permeability functions are used for both phases. The implementation of the relative permeability and capillary pressure into PFLOTRAN is shown on the documentation page. Constant density and viscosities of the phases are used by defining

TABLE I. Parameters used in 1D analytical solutions. All convergence times are from simulations on a MacBook Pro laptop with a 3.1 GHz processor and 16 GB of memory.

| Name | Model details | Grid cells to convergence (norm used) | Time to convergence |
|---|---|---|---|
| Model 1 | Injection of air into a completely saturated linear aquifer. The air and water components completely immiscible so there is no component partitioning between phases. This problem is isothermal. (BL_1D_GENERAL_IMMISC_GAS_INJ) | 400 (L2) | 44 sec |
| Model 2 | Air injection into a radial aquifer with properties identical to Model 1. (1D_RAD_BL_GENERAL_IMMISC_GAS_INJ) | 100 (L2) | 3.0 sec |
| Model 3 | Water injection into a completely dry linear porous media. The air and water components exist in both fluid phases, so there is component partitioning driven by the fluid flow. (BL_1D_GENERAL_COMP_WATER_INJ) | 100 (L1) | 5.4 min |
| Model 4 | Air injection into a completely saturated linear aquifer. The air and water components exist in both fluid phases, so there is component partitioning driven by the fluid flow. (BL_1D_GENERAL_COMP_GAS_INJ) | 40 (L1) | 18 sec |
| Model 5 | Water injection into a completely dry radial porous media with identical flow properties as Model 3. (BL_1D_RAD_GENERAL_COMP_WATER_INJ) | 80 (L1) | 3.2 min |
| Model 6 | Air injection into a completely saturated aquifer with identical flow properties as Model 4. (BL_1D_RAD_GENERAL_COMP_GAS_INJ) | 80 (L1) | 23 sec |
| Model 7 | $CO_2$ injection into a completely saturated linear aquifer. The $CO_2$ and water components exist in both fluid phases, so there is component partitioning driven by the fluid flow. (BL_1D_MPHASE_COMP_CO2_INJ) | 480 (L1) | 6.8 min |
| Model 8 | Injection of cold air into a completely saturated linear aquifer. The air and water components completely immiscible so there is no component partitioning between phases. (BL_1D_GEN_IMMISC_COLD_GAS_INJ) | 1000 (L1) | 4.2 min |

CONSTANT properties in the phase EOS sections of the input file. It is not possible to completely turn off capillary pressure, compressibility or diffusion in the simulated solution. The VAN_GENUCHTEN capillary pressure function is used with parameters chosen so that the simulated capillary pressure is negligible, and the assumptions of the analytical model are justified.

Figure 1 shows a series of simulated profiles with increasing grid refinement compared with the analytical solution. The simulator is able to capture most of the displacement even with a relatively coarse grid of 50 grid cells, but the saturation shock front is not well resolved until the grid is highly refined, to 400 grid cells. The simulation time for 400 grid cells is 44 seconds, which is surprisingly long for such a small, one-dimensional problem. This highlights the stiffness of the system of equations in the analytical solution and the small grid cells necessary to converge on the solution.

Spreading of shock fronts is intrinsic to simulating discontinuities in fluid flow models. PFLOTRAN uses single-point upstream weighting, which is known to result in a diffusion-like second-order error term in the flux approximation. However, even when higher-order methods are used, convergence to MOC solutions with saturation shocks has been shown to be at best first-order (Goater and LaForce, 2010).

The difference between the analytical and numerical solution is evaluated by using the L2 relative, or mean squared error metric:

$$L2 = \frac{\sqrt{\sum(Q^{sim} - Q^{an})^2}}{\sqrt{\sum(Q^{an})^2}} \quad (7)$$

Q is the simulation output quantity used for comparison, where $Q^{an}$ and $Q^{sim}$ denote the analytical and simulated solutions, respectively. The sum is over all the cell centers on the simulation grid. In Model 1 $Q=S_w$, is used to test for convergence.

TABLE 2. Parameters used in Models 1-6.

| Parameter | Value |
|---|---|
| Domain length (m) | 10.0 |
| Domain cross-sectional area ($m^2$) | 1.0 |
| Porosity (-) | 0.25 |
| Permeability ($m^2$) | $1.0x10^{-12}$ |
| Model 1 gas injection rate (g/s) | $2x10^{-5}$ |
| Model 2 gas injection rate (g/s) | $2x10^{-4}$ |
| Simulation time (yr) | 1.0 |
| Gas phase viscosity, $\mu_g$, (Pa-s) | $1.61x10^{-5}$ |
| Water phase viscosity, $\mu_w$, (Pa-s) | $1.00x10^{-3}$ |
| Gas phase density, $\rho_g$, ($kg/m^3$) | 1.18 |
| Water phase density, $\rho_w$, ($kg/m^3$) | $1.00x10^3$ |
| Gas phase molecular weight, (g/mol) | 28.9598 |
| Temperature ($^oC$) | 25.0 |
| $S_{wr}$ (-) | 0.1 |
| $S_{gr}$ (-) | 0.1 |
| Lambda (-) | 0.8 |
| Alpha (-) | 1.0 |

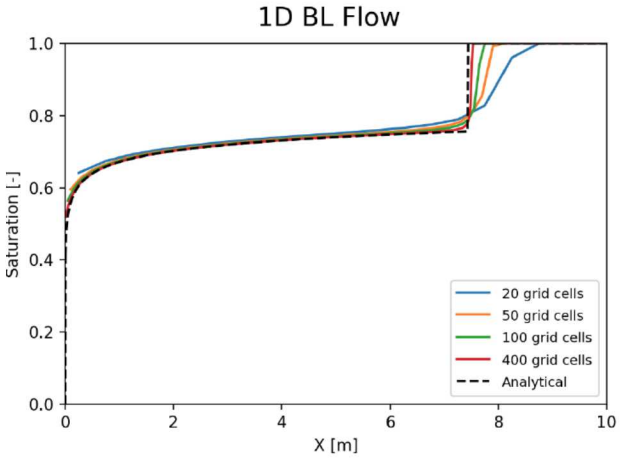


Fig. 1. Comparison of the analytical solution for Model 1 with simulations with increasing grid refinement.

A tolerance of 2% error is used by the QA test harness to test for convergence. Figure 2 shows the rate of convergence (top) and comparison plot of the converged solution (bottom) as they are generated in the QA test harness. In this example 400 grid cells were necessary for the simulation to converge within the 2% error tolerance.

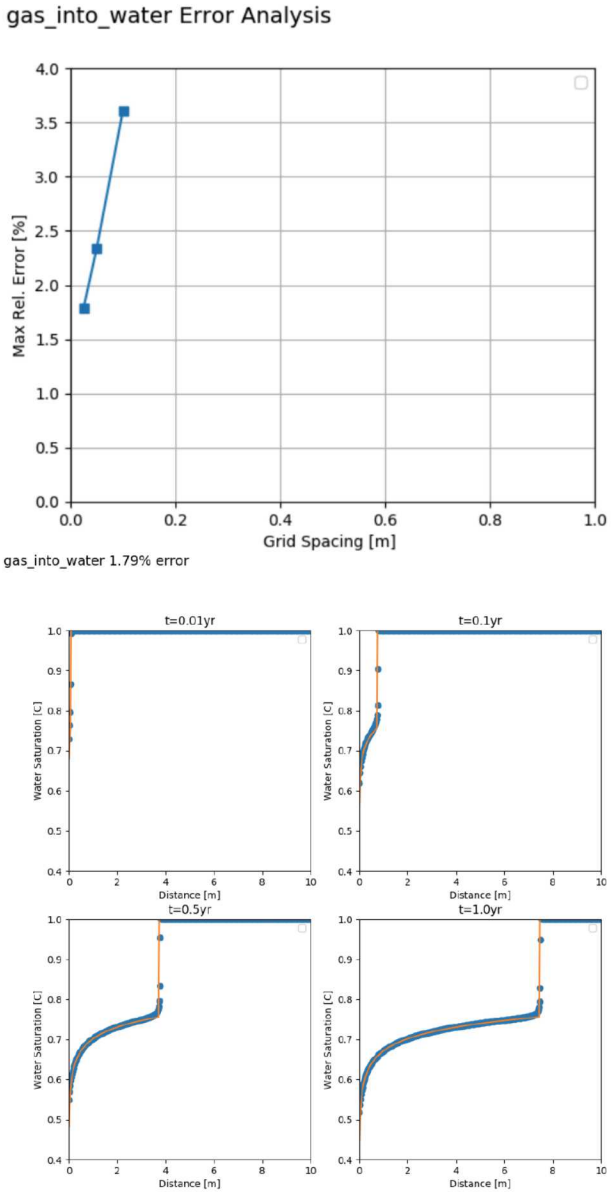


Fig. 2. Top: Rate of convergence of simulation to analytical solution for Model 1. Bottom: Comparison of the analytical solution with converged simulation for Model 1 as output by the PFLOTRAN test harness.

### I.B. Model 2: Immiscible, isothermal radial flow

This scenario describes radial flow outwards from a gas injection well in a one-dimensional radial porous medium. The governing equation for this scenario is identical to Eq. 1. The only difference in the model is that x now represents radial distance, so that the travelling

wave solution to the analytical model is proportional to $\sqrt{x}/t$ instead of x/t. Solutions are discussed in more detail in Sumnu-Dindoruk and Dindoruk (2008). Gas injection takes place at x=0, and the aquifer is modelled as 10 m long, but has an open boundary at x=10m to represent an infinite-acting radial aquifer.

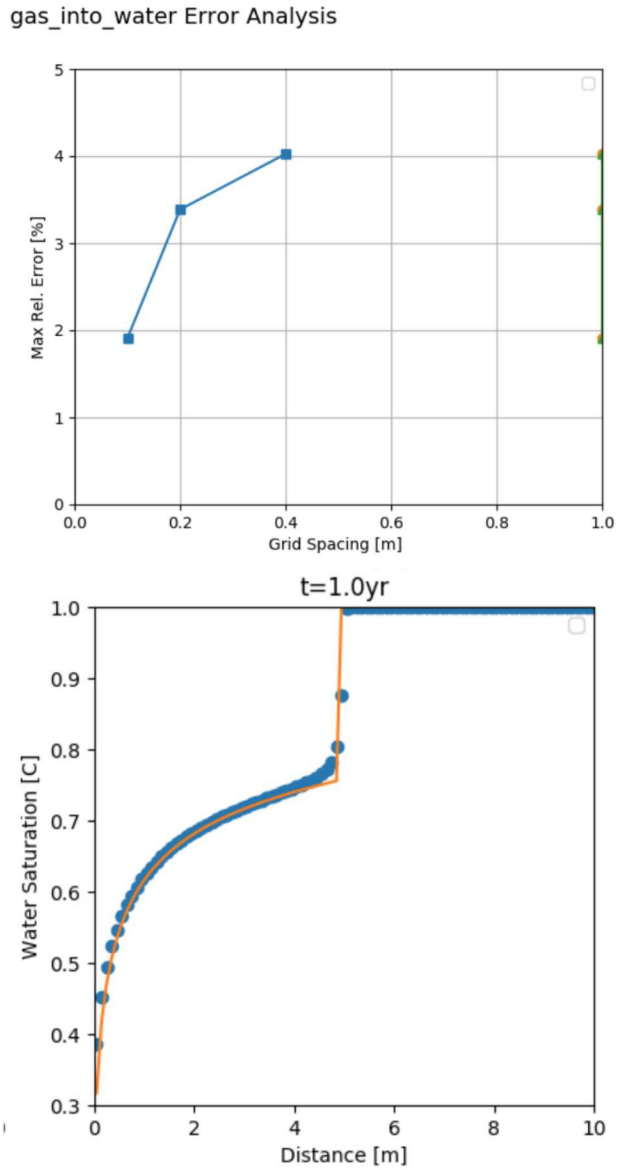


Fig. 3. Top: Rate of convergence of simulation to analytical solution for Model 2. Bottom: Comparison of the analytical solution with converged simulation for Model 2.

The properties outlined in Table 2 are used for Model 2. The only property that has changed between Models 1 and 2 is that the rate for the cylindrical problem is one order of magnitude larger. This is necessary because a radial domain of length 10m has volume $100\pi$ m$^3$, while the one-dimensional linear domain had volume 10 m$^3$.

The purpose of including this benchmark in addition to Model 1 is to ensure that the two-phase flow simulation converges on the structured cylindrical grid type.

Figure 3 shows the rate of convergence (top) and comparison plot of the converged solution (bottom) as they are generated in the QA test harness. The L2 error metric is again used to compute the error in the simulated solution. In this example 100 grid cells were necessary for the simulation to converge within the 2% error tolerance.

**I.C. Models 3 and 4: Compositional, isothermal linear flow**

These two examples add a layer of complexity to the system of equations above that considered in Models 1 and 2. These test cases consider miscible multiphase flow, meaning that the air and water chemical components both exist in the gas and liquid phases. The model in this case is as outlined in Eq. 1 with auxiliary relations in Eqs. 3 and 4. A full derivation of the analytical solution to these equations is in Section 4.4 of Orr (2007). As in the previous examples, the thermal equation is not needed because temperature is constant.

Model 3 represents water injection into a dry porous medium. The parameters used in the simulation are shown in Table 2 with additional compositional parameters in Table 3. It is important to note that the phase compositions shown in Table 3 are taken from the simulation output files, so this benchmark verifies the solutions to the flow equations, not the computations behind the air/water component partitioning. PFLOTRAN does not account for dissolved gas in calculating the liquid phase density, so the pure and mixture liquid densities are the same, while the gas phase density is a function of the phase composition, as shown in Table 3.

There may be up to two shocks in composition when the phase partitioning of components is added to MOC models as described in Eqs. 1-5 (Orr, 2007). The first shock is the water saturation shock. This is similar to the shock in saturation in Models 1 and 2, but slightly more complex because wherever there are two phases present the water phase is saturated with respect to the air component and the gas phase is fully saturated with evaporated water. This means that both the saturation and the compositions of the phases change simultaneously across the shock front.

The second shock is at the trailing end of the displacement. As it is possible for air to dissolve into the water phase, there is a trailing saturation shock where the system transitions from a two-phase state to a liquid state with an air mole fraction of zero.

Figure 4 shows the profiles for the Model 3 analytical solution and simulations with increasing levels of

refinement. The saturation and total molar concentration of each component are shown. As can be seen, across each shock in saturation the composition of the phases also changes. When two phases are present the smooth change in saturation also results in a smooth change in the component molar concentration. Downstream of the leading front there is only air component, and upstream of the trailing dissolution shock there is only water component.

TABLE 3. Additional parameters used in Models 3-6.

| | |
|---|---|
| Model 3 Henry's Law constant (1/Pa) | $5.0\text{x}10^{9}$ |
| Model 4 Henry's Law constant (1/Pa) | $1.5\text{x}10^{8}$ |
| Mole fraction of water in the gas phase, $c_{wg}$ (-) | $3.111\text{x}10^{-2}$ |
| Mole fraction of gas in the gas phase, $c_{gg}$ (-) | 0.96889 |
| Model 3 Mole fraction of water in the water phase, $c_{ww}$ (-) | 0.99998 |
| Model 3 Mole fraction of gas in the water phase, $c_{wg}$ (-) | $5.0\text{x}10^{-5}$ |
| Model 4 Mole fraction of water in the water phase, $c_{ww}$ (-) | 0.99934 |
| Model 4 Mole fraction of gas in the water phase, $c_{wg}$ (-) | $6.6\text{x}10^{-4}$ |
| Density of pure water phase (kg/m$^3$) | $9.9716\text{x}10^{2}$ |
| Density of water phase with dissolved gas (kg/m$^3$) | $9.9716\text{x}10^{2}$ |
| Density of pure gas phase (kg/m$^3$) | 1.1845 |
| Density of gas phase with evaporated water (kg/m$^3$) | 1.1720 |
| Model 3 water injection rate (g/s) | $6.0\text{x}10^{-2}$ |
| Model 4 gas injection rate (g/s) | $7.5\text{x}10^{-5}$ |
| Model 5 water injection rate (g/s) | 1.0 |
| Model 6 gas injection rate (g/s) | $7.5\text{x}10^{-4}$ |

Due to the additional complexity of the model and subsequent spreading of the shocks it was necessary to switch to a different error metric in order to demonstrate PFLOTRAN's convergence to the analytical solution in a few minutes of simulation time, as required for the QA test harness. The relative L1 norm of the difference between analytical and numerical solution is used:

$$L1 = \frac{\sum|Q^{sim} - Q^{an}|}{\sum|Q^{an}|} \tag{8}$$

|.| denotes the absolute value, $Q^{an}$ and $Q^{sim}$ denote the analytical and simulated solutions, respectively. The sum is again over all the cell centers on the simulation grid. In the compositional problem of Model 3 the phase saturation does not contain all of the information necessary to verify convergence, so $Q=C_w$, the total moles of water is used in Eq. 8.

As can be seen in Figure 4, the simulated profile again converges very quickly to the portions of the solution where the saturation and compositions are changing continuously, but the simulation spreads out the shock fronts. The simulation with 100 grid cells has converged to within 2% error of the analytical solution using the L1 norm. This simulation took 5.4 minutes to converge. By comparison, convergence using the L2 error took 320 grid cells and 51 minutes to converge to within 2% error, which is obviously far too long to include in the test harness. The long computation times are indicative of the model requiring small time steps and also the complexity introduced by allowing components to partition between the phases.

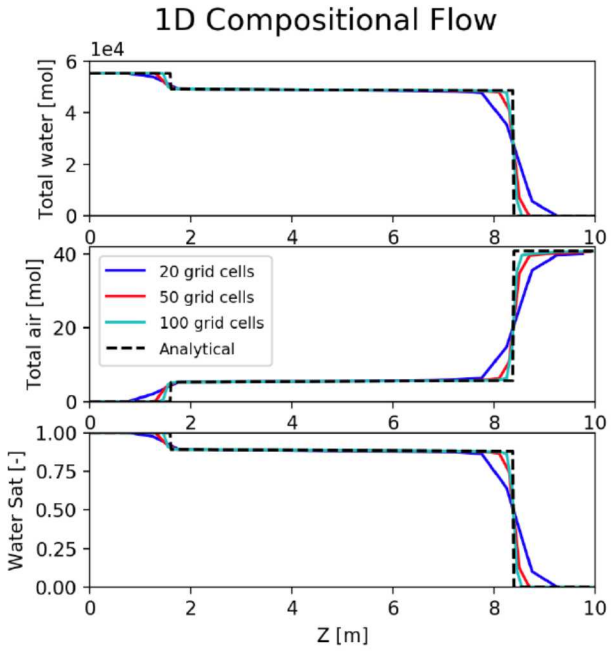


Fig. 4. Comparison of the analytical solution for Model 3 with simulations with increasing grid refinement.

Model 4 is the case of air injection into water using parameters nearly identical to Model 3, as shown in Tables 2 and 3. The only difference is an even lower mole fraction of the air component in the water phase. In Model 4 the trailing shock across which water evaporates into the gas phase moves very slowly and is not captured by either the simulation or the analytical solution projected onto the resolved simulation grid, as can be seen in Figure 5.

The Model 4 simulation converges quickly to the analytical solution using just 40 grid cells and a computation time of 18 seconds. As gas is the injected component in this case, the correct comparison quantity for convergence in Eq. 6 is the total moles of air, $Q=C_g$. This benchmark case shows that the realistic problem of

air injection into an aquifer is far easier to solve numerically than the water injection problem of Model 3 with similar parameters.

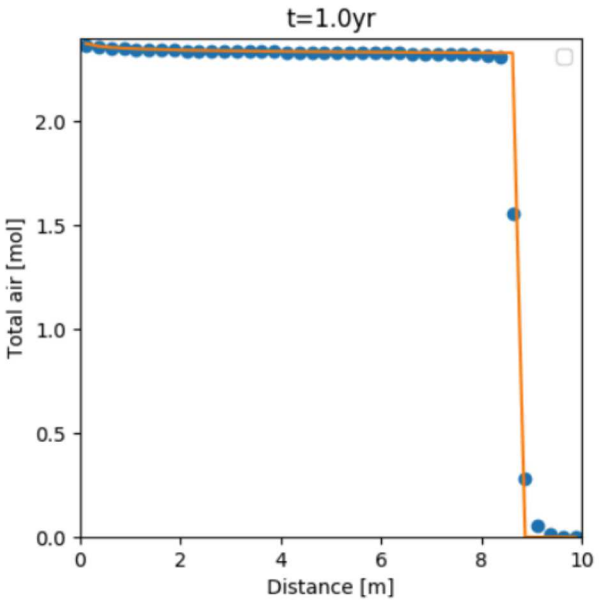


Fig. 5. Comparison of the analytical solution for Model 4 with the converged simulation.

### I.D. Models 5 and 6: Compositional, isothermal radial flow

Models 5 and 6 are the radial versions of Models 3 and 4, respectively. The results of the models are not shown as they are qualitatively similar to the results of the linear flow problems in Model 3 and 4.

Model 5 for water injection converges for the simulation with 80 grid cells, and a long computation time of 3.3 minutes. Model 6 for gas injection again converges quickly to the analytical solution in a simulation with 80 grid cells and a computation time of just 23 seconds. It is interesting in this case that the converged grid refinement is identical, but the computation times are so different.

As with the linear gas injection problem, the trailing evaporation shock in Model 6 is not captured in either the simulated solution or the projection of the analytical solution on the simulation mesh. The lack of trailing shock is almost certainly the reason that the simulation for Model 5 takes so much longer than Model 6.

### I.E. Model 7: Compositional, isothermal linear $CO_2$ flow

Model 7 is conceptually identical to Model 4. The equations to be solved are Eq. 1, with auxiliary relations Eq. 3-4. The construction of the analytical solutions is the same as Models 3-6. The computational difference is that for simulating super-critical $CO_2$ injection a full equation of state (EOS) must be solved to find the properties of super-critical $CO_2$ and $CO_2$-saturated water, whereas the previous examples the water phase properties were not dependent on the dissolved gas mass.

The PFLOTRAN module MPHASE is capable of simulating this problem. As in the previous four models, the phase composition parameters used in the analytical solutions are taken from simulation output. This benchmark does not test the accuracy of the solutions to the EOS, but rather the ability of PFLOTRAN to model the flow of water and $CO_2$ in the reservoir assuming the EOS is correct.

TABLE 4. Parameters used in Model 7 for $CO_2$ injection into an aquifer.

| Parameter | Value |
|---|---|
| Domain length (m) | 5.0 |
| Domain cross-sectional area ($m^2$) | 1.0 |
| Porosity (-) | 0.25 |
| Permeability ($m^2$) | $1.0\text{x}10^{-12}$ |
| Model 7 gas injection rate (g/s) | $8\text{x}10^{-3}$ |
| Simulation time (yr) | 0.8 |
| $CO_2$-phase viscosity, $\mu_g$, (Pa-s) | $2.8\text{x}10^{-5}$ |
| Water phase viscosity, $\mu_w$, (Pa-s) | $5.41\text{x}10^{-4}$ |
| Density of pure water phase ($kg/m^3$) | $9.92\text{x}10^{2}$ |
| Density of water phase with dissolved $CO_2$ ($kg/m^3$) | $1.00\text{x}10^{2}$ |
| Density of pure $CO_2$ phase ($kg/m^3$) | $3.79\text{x}10^{2}$ |
| Density of $CO_2$ phase with evaporated water ($kg/m^3$) | $3.85\text{x}10^{2}$ |
| $S_{wr}$ (-) | 0.1 |
| $S_{gr}$ (-) | 0.1 |
| Lambda (-) | 0.8 |
| Mole fraction of water in the $CO_2$ phase, $c_{wg}$ (-) | $1.25\text{x}10^{-3}$ |
| Mole fraction of $CO_2$ in $CO_2$ phase, $c_{gg}$ (-) | 0.99875 |
| Mole fraction of water in the liquid phase, $c_{ww}$ (-) | 0.97994 |
| Mole fraction of $CO_2$ in the liquid phase, $c_{wg}$ (-) | $2.006\text{x}10^{-2}$ |

The parameters used in the simulated and analytical solutions are shown in Table 4. They are representative of an aquifer at 50°C and 10 MPa, which corresponds to a typical 1 km depth for $CO_2$ storage. The built-in VAN_GENUCHTEN_DOUGHTY relative permeability model was used in these simulations. This is slightly different than the van Genuchten relative permeabilities used in the rest of the models.

The numerical complexity of this problem means that a highly refined grid of 480 grid cells, and a computational time of 6.8 minutes is required to have convergence to the analytical solution for $Q=C_{co2}$ to

within 2% error using the L1 error metric in Eq. 8. This is the most time-consuming test case in the QA harness. A radial benchmark case was also built, but computation times were prohibitively long for the test suite.

### I.F. Model 8: Immiscible, non-isothermal linear flow

Model 8 is for injection of cold air into an aquifer completely saturated with water. The fluid problem is assumed to be immiscible, like Model 1, however the thermal equation is now needed to solve for the temperature. The equations necessary for this example are Eq. 2 with auxiliary relation Eq. 5 for temperature and Eq. 6 with auxiliary relation Eq. 4 for the saturation profile. The construction of the analytical solution is detailed in Sumnu-Dindoruk and Dindoruk, (2008).

The fluid and thermal parameters for Model 8 are in Table 5. The phase viscosities are taken from PFLOTRAN output, so that this example verifies the solution to the flow and thermal equations, not the computations or assumptions used in the viscosity models. In Eq. 5 the product of the heat capacity times density of the injected air is much lower than the resident water or surrounding porous medium, so the thermal shock front will lag behind the saturation shock. Like the compositional flow problems in Models 3-7, there are two shocks in saturation for the non-isothermal model.

The downstream shock corresponds to the invasion of gas into the aquifer and is very similar to the leading shock in Model 1. There is no change in temperature across this saturation shock because the leading edge of the gas plume has been warmed up to reservoir temperature.

The upstream shock is where the temperature changes abruptly from the injection temperature to the initial reservoir temperature. The thermal shock also causes a change in saturation because the viscosities of the phases change between the hot and cold regions, as shown in Table 5. The simulation has to be run for 5 years, which is five times as long as Model 1, in order to resolve the slow-moving thermal shock.

The fluid flow part of the solution has already been extensively tested in the previous examples, so the L1 error in Eq. 8 is calculated using the temperature profile, so that Q=T. As shown in Figure 6, the thermal front and associated shock in saturation both suffer from numerical dispersion except for a highly refined grid. This is in large part because the thermal shock is moving very slowly relative to the leading saturation shock, which has exited the simulation domain. Model 8 requires 1000 grid cells and 4.2 minutes to converge to within the 2% error tolerance.

A radial benchmark and one for hot fluid injection were also considered, but computation times were prohibitively long to include in the test harness.

TABLE 5. Parameters used in Model 8 for cold air injection into an aquifer.

| Parameter | Value |
|---|---|
| Domain length (m) | 10.0 |
| Domain cross-sectional area ($m^2$) | 1.0 |
| Porosity (-) | 0.25 |
| Permeability ($m^2$) | $1.0x10^{-12}$ |
| Gas injection rate (g/s) | $5x10^{-3}$ |
| Simulation time (yr) | 5.0 |
| Hot gas phase viscosity, $\mu_g$, (Pa-s) | $2.54x10^{-5}$ |
| Hot water phase viscosity, $\mu_w$, (Pa-s) | $1.34x10^{-4}$ |
| Cold gas phase viscosity, $\mu_g$, (Pa-s) | $1.82x10^{-5}$ |
| Cold water phase viscosity, $\mu_w$, (Pa-s) | $1.00x10^{-3}$ |
| Gas phase density, $\rho_g$, ($kg/m^3$) | 1.18 |
| Water phase density, $\rho_w$, ($kg/m^3$) | $1.00x10^3$ |
| Solid phase density, $\rho_s$, ($kg/m^3$) | $2.70x10^3$ |
| Gas phase molecular weight, (g/mol) | 28.9598 |
| Injection temperature (°C) | 20.0 |
| Initial temperature (°C) | 200.0 |
| $S_{wr}$ (-) | 0.1 |
| $S_{gr}$ (-) | 0.1 |
| Lambda (-) | 0.8 |
| Alpha (-) | 1.0 |
| Heat capacity of gas (J/kg C) | $6.04x10^5$ |
| Heat capacity of water (J/kg C) | $4.15x10^3$ |
| Heat capacity of rock (J/kg C) | 0.01 |

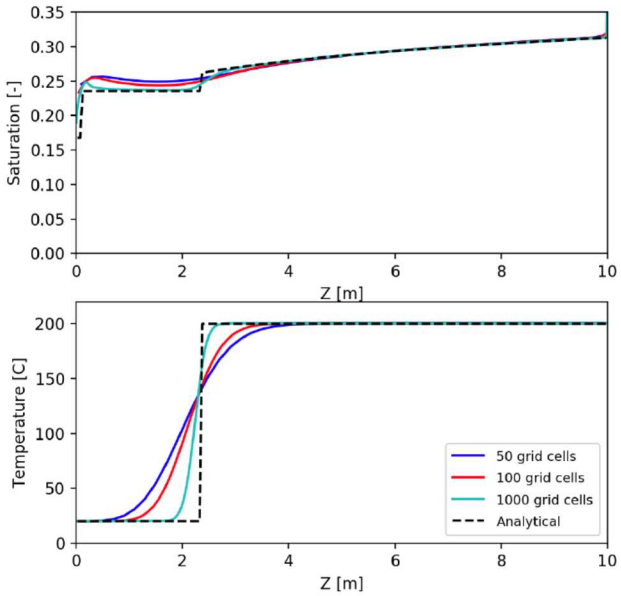


Fig. 6. Comparison of the analytical solution for Model 8 for cold gas injection with simulations with increasing grid refinement.

## IV. CONCLUSIONS

In conclusion, eight benchmark simulations in PFLOTRAN have been verified against analytical solutions. The benchmark solutions are all one-dimensional flow problems that test the ability of the simulator to converge to analytical solutions with increasingly complex phase behavior. In each case PFLOTRAN converges to within 2% of the analytical solution based on a rigorous error metric. This demonstrates that the implementation of the equations for these models are correct in PFLOTRAN, and also that the approximation in the numerical method is highly accurate when sufficient grid resolution is used. All of the presented benchmarks are freely available online as part of the PFLOTRAN test harness.

Four of the cases converge in under a minute, while the other four cases take several minutes for the simulated profile to converge to the analytical solution. Three of the displacements with more than one discontinuity in the saturation solution (Models 3, 5, and 8) have slow convergence, along with Model 7, which has a full equation of state for the fluid properties.

Models 3 and 5 do not require an unduly large number of grid cells to converge, with 100 and 80 grid cells in the final solution, respectively. These two simulations are slowed down because small timesteps are required to capture two shocks in saturation. Models 7 and 8 are slowed purely by the complexity of the phase behavior. This is a testament to the numerical stiffness of the equations in the analytical model, which have no dispersive or compressible terms, and not necessarily a reflection of computation times for more realistic problems.

## ACKNOWLEDGMENTS

This paper is Sandia publication SAND2019- 902065. Sandia National Laboratories is a multi-mission laboratory managed and operated by National Technology and Engineering Solutions of Sandia, LLC., a wholly owned subsidiary of Honeywell International, Inc., for the U.S. Department of Energy's National Nuclear Security Administration under contract DE-NA-0003525.

## REFERENCES

1. Goater, A. L., and LaForce, T. (2010, September). *Multicomponent Multiphase Transport Solutions for Application to $CO_2$ Storage*. In ECMOR XII-12th European Conference on the Mathematics of Oil Recovery.
2. Lake, L. W. (1989). *Enhanced oil recovery*. Upper Saddle River, NJ. Prentice Hall
3. Lichtner, P. C., Hammond, G. E., Lu C., Karra, S., Bisht, G., Andre, B., Mills, R. T., Kumar, J., and Frederick, J. M., (2017) PFLOTRAN Web pages accessed Jan 7, 2018: http://www.pflotran.org, and https://qa.pflotran.org
4. Mariner, P. E., E. R. Stein, J. M. Frederick, S. D. Sevougian and G. E. Hammond (2017). Advances in Geologic Disposal System Modeling and Shale Reference Cases. SFWD-SFWST-2017-000044, SAND2017-10304 R. Sandia National Laboratories, Albuquerque, New Mexico.
5. Oberkampf, W. L., and T. G. Trucano (2007), Verification and Validation Benchmarks, SAND2007-0853, 67 pgs., Sandia National Laboratories, Albuquerque, NM.
6. Orr, F. M. (2007). *Theory of gas injection processes* (Vol. 5). Copenhagen: Tie-Line Publications.
7. Sumnu-Dindoruk, D. M., and Dindoruk, B. (2008). *Analytical solution of nonisothermal Buckley-Leverett flow including tracers*. SPE Reservoir Evaluation & Engineering, 11(03), 555-564